NUMERICAL AND EXPERIMENTAL ANALYSIS OF THE EFFECT OF A PUSHER PROPELLER ON A WING

F.M. CATALANO M.Sc Ph.D Ceng MRAeS and
M.G. MAUNSELL M.Sc Ph.D AMRAeS
Aircraft Laboratory EESC - University of Sao Paulo Brazil

ABSTRACT

. This work presents a numerical and experimental analysis of the effect of a pusher propeller on a wing. The numerical analysis was divided in two parts: 1) application of the classical propeller theory to a three-dimensional panel method computer programme for the prediction of the effect of a pusher propeller on a wing/body combination, and 2). a similar application of the propeller theory to a two-dimensional panel method programme which includes boundary layer calculations. Experimental work was also performed using two different models: a half model which included fuselage, wing with a propeller placed behind it, and a two-dimensional wing with a downstream propeller. Relative position between propeller and wing could be changed in both models and a total of 9 positions for the half model and 7 positions for the two-dimensional model were analysed. Measurements included C_L, C_D, C_M, pressure distribution and boundary layer characteristics by Flow visualization. Results showed that the pusher propeller inflow affects the wing characteristics by changing lift, drag and pitching moment, and also may delay boundary layer separation. These effects are highly dependent of the relative position on wing/propeller. Both theoretical methods can predict well the effect of the propeller and can be used for designing a similar configuration.

NOMENCLATURE

a	propeller inflow factor
$b_{1/2}$	half the width at half depth in turbulent jet theory
c	wing chord
C_T	thrust coefficient
C_D	drag coefficient
C_{Di}	induced drag coefficient
C_L	lift coefficient
C_{Lmax}	maximum lift coefficient
$C_{mc/4}$	quarter chord pitching moment coefficient
J	advance ratio
L'	laminar separation point
R	reattachment point
R_1	slipstream radius of a isolated propeller
Rd_1	local displaced slipstream radius
R_p	propeller radius
$R1_{lo}$	slipstream radius at the lower surface
$R1_u$	slipstream radius at the upper surface
RHS_i	right hand side vector of panel *i*
S	separation point
S_f	frontal area of the wing immersed in the slipstream
T	transition point
U_{si},W_{si}	axial and vertical velocities induced by the wake sinks at panel *i*
Vpp	propeller local induced velocity
Vps	local velocity induced by source distribution
Vpm	local velocity induced by vortex distribution
s_P	source strength on local panel
np	unit normal to local panel
V_{ni}	transpiration velocity at panel *i*
V_∞	free stream velocity
V_{px},V_{pz}	axial and vertical velocities induced by the propeller inflow
Vt_i	tangential velocity at panel *i*
Xp,Zp	axial and vertical distances from the propeller
α	model incidence angle
θ	panel inclination
σ	free constant in turbulent jet flow
χ	free constant
ε_τ	virtual kinematic viscosity

INTRODUCTION

During the 80's a large number of works[1-4] on UDF (unducted fans) or propfans brought attention back to the non conventional configurations such as the pusher propeller. All these works pointed to the potential benefits in fuel efficiency and cabin noise from using an advanced propeller in a pusher configuration. Despite the fact that attention on propofans has decreased there is still great interest in the use of the pusher propeller configuration in general aviation[7] and commuter[2,4,8] aircraft as well as in RPV and unmanned aircraft[5]. For these classes of aeroplane the distance between the wing and the pusher propeller can be close enough to induce quite large effects on the wing surfaces, especially when the propellers are operating at high thrust as in take-off and climb. At take-off the aircraft speed is close to stall velocity and the whole process from rotation to climb-out involves a large range of incidence with the propeller

operating all the time at maximum thrust. Therefore, the effect of the pusher propeller inflow on the wing in this situation is of considerable magnitude.

This paper describes two theoretical and experimental approaches to the analysis of the problem of wing/pusher-propeller interference.

The first method involves the inclusion of a relatively simple description of the propeller effect using Koning's[10] propeller influence theory within a three dimensional first order potential flow panel method[13,14], using for comparison experimental data obtained in wind tunnel tests of a large wing-fuselage half model (**Fig. 1**) accompanied by a propeller driven by a variable frequency electric propulsion unit within a streamlined nacelle placed at several positions behind the wing (**Table 1**).

The second method concentrated on testing the effect of a high thrust pusher propeller driven by a hydraulic motor on a two-dimensional wing at a wide range of incidence and with the propeller also positioned at several positions (Table 2) behind the wing (**Figs 2** and **3**). In order to predict more accurately the wing's flowfield, a semi-inverse computer programme[9] was used in conjunction with Koning's theory in a similar manner to that used by the first method.

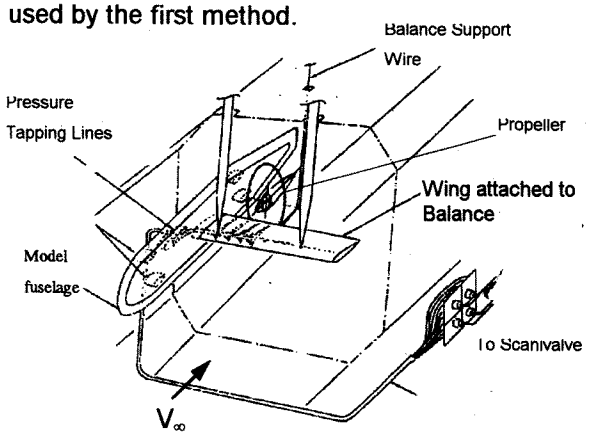

Figure 1 Half Model in the Wind Tunnel

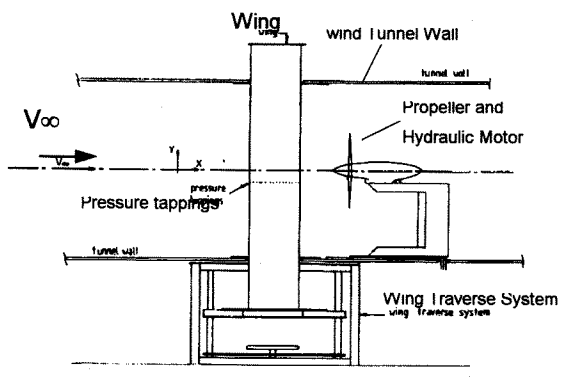

Figure 2 Pressure Measurements, Two-dimensional wing

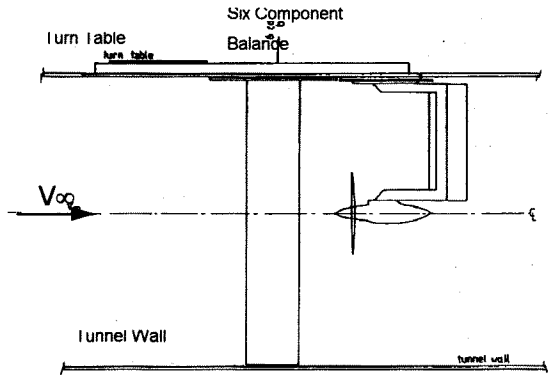

Figure 3 Force and Moment Test Set-up for the Two Dimensional wing

Table 1 Propeller Positions for the Half Model

Propeller Position	A	B	C	D	P1	P2	P3	P4	P5
Distance from wing TE (cm)	15.0	15.0	15.0	52.1	25.4	25.4	25.4	25.4	25.4
Distance of axis above(+) or below(-) wing TE	0.75	10.9	-9.4	13.5	10.9	10.9	10.9	10.9	10.9
Distance of axis from body centre-line (cm)	50.8	50.8	50.8	50.8	50.8	58.4	66.0	81.3	96.5

Table 2 Propeller Position for the Two Dimensional model

Propeller Position	POS 01	POS 02	POS 03	PSO 04	POS 05	POS 06	POS 07
Distance From TE	**0.5C**	**0.5C**	**0.5C**	**0.85C**	**0.85C**	**0.85C**	**0.5C**
Above + below - chord	**0.0**	**0.23C**	**0.46C**	**0.46C**	**0.23C**	**0.0**	**0.19C (-)**

TEST CONDITIONS

Half Model: The full scale flight operating conditions were simulated within certain limits in the tunnel. Three basic regimes were considered and are referred in general terms as Take-off, Climb and Cruise. The choice of nominal values for the tunnel freestream velocity $V\infty$ and the propeller parameters, J and C_T depended to some extent upon the experimental performance of the model propeller used. However, initial values were calculated on the basis of a full scale study. For the cruise regime, the model propeller advance ratio was set at J = 0.74 with a thrust coefficient C_T = 0.017 and for the Take-off regime: J = 0.14 and C_T = 0.095. The investigation of wing surface static pressure was limited to a general area of the wing body model centred on the wing surface between the root and approximately 50% of the semi-span of the model. The model wing was of rectangular planform, with a constant section NASA GA(W)-1 airfoil and possessed no dihedral or twist. The wing aspect ratio was 8 and the its incidence angle was set at 3.45°. Since the fuselage was solidly fixed to

the wind tunnel wall, the wing was suspended independently from the wind tunnel balance arms. Model propeller thrust grading in two diametric directions was performed for incidences angles between 0° and 20° by using the airflow total head measurements close behind the propeller blades.

Two-dimensional Model: A Wortmann FX53-137 profile wing with a chord of 0.34m was used for the tests. The wing carried 82 pressure tapping around the centre line chord. A 0.52m diameter three blade propeller driven by a 20 hp hydraulic motor was used. For the pressure measurements a 8x4 ft open return low speed wind tunnel was used with the wing positioned vertically in the working section (**Fig. 2**). The propeller was mounted in a separated pylon which could be moved in order to set the propeller/wing positions. The wing could be moved vertically through the working section in order to measure the spanwise effect of the propeller on the surface pressure distribution. The force and moment measurements were made in a 8x6 ft closed-circuit low speed wind tunnel using a similar arrangement for the propeller to that described above. The wing was attached vertically to a six component balance and spanned the tunnel except for a 3mm gap at one end so that force measurements could be made (**Fig. 3**). Flow visualisation was carried out using both sublimation and oil technique. The seven wing/propeller position were tested through the incidence range of -4 to +20 degrees with and without a trip wire. Wing surface pressure distribution were taken at 10 spanwise positions. The Reynolds number was set at 0.45 millions and the propeller was run at a thrust coefficient of C_T = 0.15 with an advance ration of J = 0.33. These propeller characteristics were chosen in order to simulate a high power condition such as take-off and climb.

KONING'S THEORY

Koning used Froude's actuator disk concept for the propeller as a simple and effective simulation that would yield the necessary steady state flow effects on adjacent solid surfaces and on the surrounding airflow. He employed what may be termed the pressure doublet, defined by Riemann[15], distributed uniformly over the disk and thus determined the flow velocity and direction within the slipstream upstream and downstream of the propeller. The same potential flow definition of the velocity within the slipstream was employed by both the above methods, given by:

$$Vp_X = a\left(1+\frac{X_P}{\sqrt{(R_P/c)^2+X_P^{\,2}}}\right) \qquad (1)$$

$$Vp_Y = -\frac{1}{2}a\frac{(R_P/c)^2 Y_P}{\sqrt{((R_P)^2+X_P^{\,2})^3}} \qquad (2)$$

$$Vp_Z = -\frac{1}{2}a\frac{(R_P/c)^2 Z_P}{\sqrt{((R_P/c)^2+X_P^{\,2})}} \qquad (3)$$

$$a = \frac{1}{2}\left(-1+\sqrt{1+\frac{8}{\pi}\frac{C_T}{J^2}}\right) \qquad (4)$$

The first method used all the above equations, however, in the second method only Vp_X and Vp_Z were determined, as a two-dimensional strip theory was applied in conjunction with the application of the Williams' viscous-inviscid interaction method[9], as the work centred on the analysis of the boundary layer and its behaviour .

In the first method, the determination of the flow velocity induced by the propeller outside the slipstream followed Koning's original logic, however a modification was introduced to avoid the use of Koning's basic assumption of a parallel slipstream of constant diameter as basis for the determination of the expression for the velocity outside the slipstream, which was necessary at the time due to the natural limitations of an analytical approach. This simplified model was substituted by a more exact model based on the real slipstream geometry, as defined by Koning later in the same work using continuity, the velocity thus becoming a function of the latter, and the x co-ordinates of the position under consideration and of the point X_R at which a line joining this point to the centre of the propeller disk cuts the slipstream frontier. Thus, where Koning's original expression for the radial velocity induced by the propeller outside the slipstream was:

$$Vp_r = -\frac{1}{2}a\frac{(R_P/c)^2 r_P}{\sqrt{((R_P/c)^2+X_P^{\,2})^3}} \qquad (5)$$

the modified form developed from the above mentioned theoretical approach was:

$$VP_r = -\frac{1}{2}a\frac{(R_P/c)^2 r_P}{\sqrt{(r_P^{\,2}+X_P^{\,2})^3}}\left[\frac{(R_1/c)^2+X_R^{\,2}}{(R_P/c)^2+X_R^{\,2}}\right]^{3/2} \qquad (6)$$

where R_1 is the local slipstream radius at X_R the X co-ordinate of the point at which a line joining (x,y,z) to the centre of the propeller disc cuts the slipstream frontier. This was naturally transformed into three equivalent orthogonal components for compatibility with the system used by the panel method computer programmes. For the analysis of the flow upstream of the propeller, consideration of the propeller downstream slipstream and its

constituent wake vortex geometry was unnecessary, as stated by Koning [10].

In the second method, the discontinuity between the flow inside and outside the slipstream is not present because a process of mixing smoothes out the transition in a similar way to that found in turbulent jets and wakes. In order to find a practical solution to the problem, it was assumed that the propeller inflow would behave as a `reversed' turbulent jet flow with a maximum velocity at the centre of the jet given by equations (1) and (3). Thus, the equations for a turbulent jet could be adapted, and after a coordinate transfer to the global panel coordinates, the velocities were given by:

$$Vp_{X,Z} = (Vp_{X,Z})_{Koning} (1 - \tanh^2 \eta) \qquad (7)$$

where

$$\eta = \sigma \frac{Y_P}{X_p} \quad with \quad \sigma = \frac{1}{2}\sqrt{\frac{Vp_{X,Z}\ X_P}{\varepsilon_\tau}} \qquad (8)$$

The virtual kinematic viscosity ε_τ is a function of the width of the jet and of the centre line velocity, and is given by:

$$\varepsilon_\tau = \chi\ b_{1/2}\ (Vp_{X,Z})_{Koning} \qquad (9)$$

The free constant χ was determined experimentally following Schlichting's[11] methodology. The width of the jet was assumed equal to the slipstream radius at the wing surfaces and wake. Slipstream radius was calculated assuming that by continuity the volume flow through the slipstream must remain the same for both the isolated propeller and for a propeller with a wing in front, so that we have:

$$\pi Rd_{1\,i}^2 - S_{f_i} = \pi R_{1\,i}^2 \qquad (10)$$

$$with \quad S_{f_i} = \frac{1}{2}\ t_i \left(2\,R_{1U_i} + 2\,R_{1LO_i}\right) \qquad (11)$$

$$R_{1LO_i} = \sqrt{R_1^2 - \left(Z_P - t_{LO_i}\right)} \qquad (12)$$

$$R_{1U_i} = \sqrt{R_1^2 - \left(Z_P - t_{u_i}\right)^2} \qquad (13)$$

Where ***ti*** is the local aerofoil thickness and R_{1U} and R_{1LO} are functions of the propeller position. Equation **(10)** is a polynomial in Rd_1 from which only the real and positive root was taken in order to find the slipstream boundary. Without the propeller effects the ***RHS*** vector of the system of equations which calculates the strength of the unknowns is formed by the normal components of $V\infty$ and the normal velocities from the wake sinks and vortices for the inviscid solution, plus the transpiration velocity from the viscous calculation. With the propeller effects, the ***RHS*** vector becomes:

$$(RHS_i)_{ON} = (RHS_i)_{OFF} + VP_{X_i} \sin\theta_i + VP_{Z_i} \cos\theta_i \qquad (14)$$

and the tangential velocity at the control point of the panel i determined after the system reaches a satisfactory convergence is given by:

$$(Vt_i)_{ON} = (Vt_i)_{OFF} + VP_{X_i} \cos\theta_i + VP_{Z_i} \sin\theta_i \qquad (15)$$

The two-dimensional calculations were performed in strips in the spanwise direction and the results were integrated along the span in order to obtain the overall effect of the propeller inflow on the wing.

GENERAL THEORETICAL PROCEDURES

First Method - The basic `programme packet' into which the propeller effect was introduced consisted of a combination of two computer programmes: a `model geometry programme', which arranges the input data describing the complete geometry of the model wing-fuselage configuration into a convenient form for the subsequent analysis of the aerodynamic flow over the model surface by the second, `aerodynamic calculation programme'. The size (radius) of the propeller , its position with respect to the coordinate system of the wing-fuselage, and velocity ratio ***J*** and thrust coefficient C_T were added to the normal geometric input data for this programme, however the calculations of the induced velocity due to the effect of the propeller at each panel collocation point were performed in the second programme, within which the calculations of the propeller influence were added to the main programme body, rather than added as a sub-routine.

The panel method used is a first order potential flow method based on that developed by Kraus[13] and improved by Butter[14] using surface panels with uniform source distribution and internal discrete vortex sheets positioned on the mean camber surface within the wing, extending out at the trailing-edge as a flat trailing vortex sheet set at the angle governed by alignment with the semi-angle formed by the final upper and lower trailing-edge panels of each wing section along the wing span, as well as within the fuselage at the wing - fuselage intersection.

The additional flow velocity component due to the propeller or propellers was added to the freestream velocity component at each panel collocation point, giving a total velocity at each panel of:

$$\bar{V}_P = \bar{V}_\infty + \bar{V}_{PP} + \left[\sum_{1}^{N-1} \bar{V}_{P_S} + \sum_{1}^{N} \bar{V}_{P_m}\right] + \frac{1}{2}\sigma_P \bar{n}_P \qquad (16)$$

Second Method - Full details of the computational programme used in the second method for the calculations of the aerodynamic characteristics of the wing are given in the paper by Williams[9]. The programme uses an integral boundary layer method which has been extended to calculate separated flow by assuming a two parameter description of the separated velocity profiles. The programme uses an integral boundary layer method which has been extended to calculate separated flow by assuming a two parameter description of the separated velocity profiles. The programme is of the semi-inverse type in which a direct inviscid calculation is coupled to an inverse calculation of the boundary layer. The outer inviscid flow is assumed here to be both incompressible and irrotational, so that it can be described by the relevant solution of Laplace's equation, which is obtained by a surface singularity method. In the inner viscous flow, the laminar portion of the boundary layer is calculated by Thwaites' method and natural transition is predicted using Granville's correlation. If laminar separation occurs before transition, then the laminar separation bubble is calculated using Horton's semi-empirical technique. The development of the turbulent boundary layer and wake is calculated by the inverse formulation of Green's lag-entrainment method. The axial and vertical velocities induced by the propeller inflow inside the slipstream, as given by Koning's theory, were included in the inviscid calculations of the programme.

RESULTS

Experimental results for the half model: For the low power case the experimental chordwise pressure distribution are shown in **Figure 4** and **5** for two propeller positions: B and C. For this case the pressure distribution shown in Figures 4 and 5 is nearly unchanged to the first order from the no-propeller case and is not a function of propeller position. The curves of thrust grading are shown in **Figure 6** and **Figure 7** for propeller positions B and C . The results show a greater effect on the blade loading when the propeller disk crosses the wing wake as in position B. The propeller/wing interference at High power and low propeller advance ratio is large and, unlike the low power case, the lift coefficients are more than doubled in the region of the wing span directly influenced by the propeller as it can be seen in **Figure 8** . The effect of the wing on the propeller thrust grading is, however, very small and the thrust distribution is almost symmetrical about the propeller axis (**Figure 9**).

Two-dimensional Wing: Figure 10 shows the pressure distributions at the centre line of the wing at various incidence angles compared with the propeller-off case. Also is showed in Figure 11 the C_L-α and C_L - C_D curves for propeller position 03 compared with propeller-off case. The increase in suction in the upper surface of the wing due to the propeller is clearly shown on the pressure distributions of Figure 10, this resulted in a gain in C_L as shown in the C_L-α curve of Figure 11. The effect of the propeller is larger at the working incidence angles (-4 to 6 degrees) for propeller positions above the wing's chord line and close to the trailing-edge as can be seen in the normal force coefficient distribution of Figures 12 and 13. An direct consequence of this increase of suction in the upper surface of the wing is an increase of pressure drag as shown in the C_L - C_D curve of Figure 11. However, L/D performance of the wing has improved for most of the propeller position with best results for position 03. At high incidence angles part of this gain in C_L is due to a delay in turbulent separation as demonstrated by the movement downstream of the separation point S in the $\alpha = 12.5^{\circ}$ curve of Figure 10. The spanwise effect of the propeller on turbulent separation determinated by oil flow visualisation is shown in Figure 15. When using a smooth surface wing the general effect of the propeller on the aerodynamic characteristics of the wing is similar to that of the rough wing case as can be seen in **Figures 16** and **17**. Because the boundary layer transition, in this case is free from any trip, and also due to the low Reynolds number of the experiment, the effect of the propeller on changing local flow incidence affects the transition front. This effect can be seen in Figure 16 by the movement of the transition point T (determinated by sublimation). This effect decrease after incidences angles grater than 8 degrees as shown in Figure 18 for the propeller position 01.

Numerical Results: The results of the first method shown here in Figure 19, refer specifically to the wing loading, comparing experiment and theory and showing disagreement particularly in the wing root area for propeller positions close to the root probably partly due to viscous effects in this region in which boundary layer interaction with the propeller induced flowfield is likely to be accentuated, and partly due to the limitations imposed by the simplicity of the geometry of the propeller slipstream model. The latter adhered to that defined by Koning's original theory, for a propeller alone in a freestream flow normal to the propeller disc. The theoretical model thus assumed a slipstream with a circular cross-section and a straight axis normal to the propeller disc which remained in this form, even when penetrated by the wing. Inaccuracy of the theoretical flowfield was thus accentuated on the wing surface within and close to the propeller slipstream, becoming surprisingly close to the experimental results for

positions outside or nearly outside the propeller slipstream, as can be seen for propeller positions P4 and P5. In fact this work showed surprisingly close results, in terms of section C_L when considering the relatively high propeller disk loading,(C_T = 0.095), for the high power case, considering Koning's use of small perturbation theory in his derivation of the basic equations and his later declaration that in most cases the disturbance velocity, due to the action of the propeller be small compared to the freestream velocity. The explanation for this perhaps rests on the fact that a numerical approach allows the local perturbations in the airflow to be considered in incremental form and applied to separate surfaces, thus minimising the consideration of larger perturbations during the calculation.

The results of the second method show in Figures 20 and 21, the comparison of experimental chordwise pressure distributions with theory for α= 7.5° and α= 12.5° for the wing with a trip wire. The results are quite good for most of the spanwise stations despite discrepancies at the suction peak due to the presence of the trip wire. Figure 22 shows that the lift coefficient calculated by integrating the theoretical pressure distribution in the spanwise direction can satisfactorily predict the effect of the propeller inflow on the wing. The theoretical results agree well with the pressure distribution for the wing with smooth surfaces, as can be seen in Figure 23. Transition and turbulent separation on the smooth wing can also be predicted by theory, as shown in Figure 24. The theoretical method for this Reynolds number, always indicates transition involving a laminar separation bubble, whereas in the experiment the transition is natural between α = 6° and α = 14°.

CONCLUSIONS

The effect of a pusher propeller on the flow over a wing/body combination and a straight wing was investigated by wind tunnel tests and numerical methods. A total of 16 different configurations of the models were investigated. The propeller induced flow over the models surfaces, thus increasing Lift, pressure drag, pitching moment and delaying turbulent separation. The propeller effect was more intense on the rear of the wing but can also extend to the front by changing upwash angle. The propeller effects are very dependent on the propeller/wing relative position. Over the working range of incidence angles, propeller positions above the wing gave best results. The propeller inflow can also delay transition by preserving laminar flow in a smooth wing at low Reynolds number due to the alleviation of adverse pressure gradient at the rear of the wing. The first method in its present form showed promise as a method of assessment of the aerodynamic characteristics of a multi-engined pusher propeller wing-body configuration and particularly in the design mode as a means of indicating suitable propeller positions for a given layout.

A potential exists for much further theoretical work including a more exact representation of the propeller slipstream geometry and the use of a non-uniformly loaded actuator disc which better simulates real propeller loading under the influence of a non-uniform inflow. Work has already been done on the inclusion of the downstream propeller wake and the analysis of the interaction of the latter with other flying surfaces, using the same panel programmes as a basis. There is also room for further work in the area, including relaxation of the propeller wake for instance.

The second method showed that the Williams semi-inverse computer programme in conjunction with Koning's theory gave good results for the centreline pressure distribution. The spanwise effect of the propeller inflow simulated by adapting the turbulent jet flow equations, also gave good agreement with experimental results. The flow over the wings in a pusher configuration operating at low Reynolds, can also be well predicted despite the difficulties with transition point calculations.

REFERENCES

1. **Henne P.A., Dahlin J.A., Peavey C.C., Gerren D.S.**-Configuration design Studies and Wind Tunnel Tests of an Energy Efficient Transport with a High Aspect Ratio Supercritical Wing , NASA CR-3224, May, 1982.
2. **Goldsmith, I.M.**- A Study to Define the research and Technology Requirements for Advanced Turbo/Propfan Transport Aircraft. NASA CR-166138, 1981.
3. **Dunham, D.M., Gentry, G.L.Jr., Gregory M.S., Applin, Z.T. and Quinto P.F.**- Low Speed Aerodynamic Characteristics of an Twin-Engine General Aviation Configuration with Aft-Fuselage-Mounted Pusher Propellers. NASA TP-2763, 1987.
4. **Coe P.L. Jr., Turner S.G. and Owens D.B.** - Low Speed Wind Tunnel Investigation of the Flight Dynamics Characteristics of an Advanced Turboprop Business/Commuter Aircraft Configuration. NASA TP-2982, 1990.
5. **Catalano, F.M. and Stollery J.L.** - The Effect of a High Thrust Pusher Propeller on the Aerodynamic Characteristics of a Wing at Low Reynolds. ICAS - 94-6.1.3, Anahein California USA September 1994
6. **Catalano, F.M.** - The Effect of a High Thrust Pusher Propeller on the Flow over a Straight

Winw. Ph.D Theses, College of Aeronautics Cranfield University, England 1993.
7. **Maunsell, M.G.**- A Study of Propeller/wing /body Interference for a Low Speed Twin-Engined Pusher Configuration. ICAS-90-5.4.3, 1990.
8. **Johnson J.L. and White E.R.**- Exploratory Low Speed Wind Tunnel Investigation of an Advanced Commuter Configuration Including an over-the-wing Propeller Design. AIAA-83-2531, 1983.
9. **Wlliams B.R.**- The Prediction of Separated Flow Using a Viscous-Inviscid Iteration Method. R.A.E. Tech. Memo. Aero 2010, Farnboroug. Dec. 1984.
10. **Koning C.**- Influence of the Propeller on the Other Parts of the Aeroplane Structure. Div. M Aerodynamic Theory, Vol. IV, Edited by Durand W., CIT Cal 1935.
11. **Schlichting H.**- Boundary Layer Theory. McGraw-Hill, Inc, 1979.
12. **Glauert H.** - The Elements of Airfoil and Airscrew Theory. Second Edition, Cambridge University Press 1947.
13. **Kraus W-** Panel Methods in Aerodynamics Chapter 4- Numerical Methods in Fluid Dynamics, Edited by Wirz H.J., Smolderen J.J.- Von Karman Inst. For Fluid Dynamic, Hemisfere Publishing Corp. McGraw Hill, 1978.
14. **Butter D.J.** - Program Specification for the MBB Panel Method, Hawker Siddeley Aviation Ltd. Report No. HSA-MAE-R-CMP-0007, July 1977.
15. **Riemamm-Webers-** Differentialgleichumgerder Physik. Vol I, Chapt. XIV, Braunschareig, 1925.

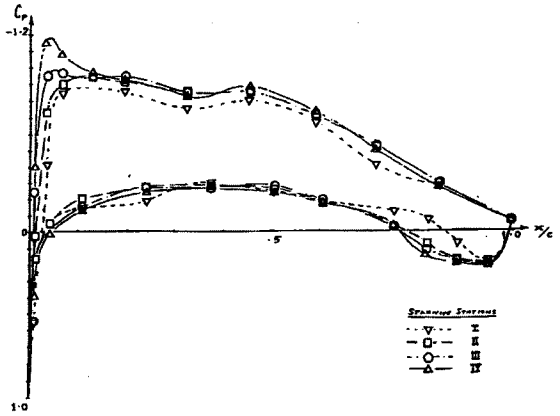

Figure 4 Experimental Chordwise Pressure Plots, Propeller Position B, Low power Case

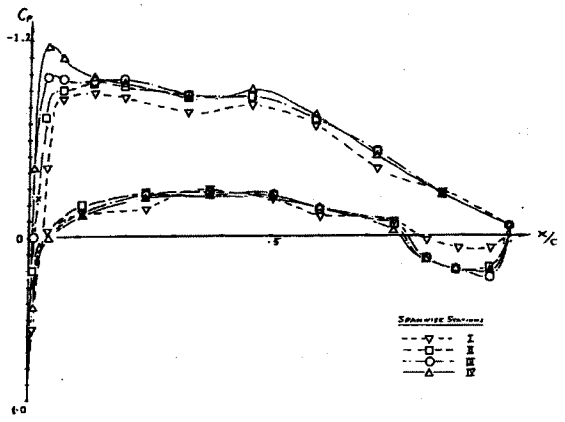

Figure 5 Experimental Chordwise Pressure Plots, Propeller Position C, Low Power Case

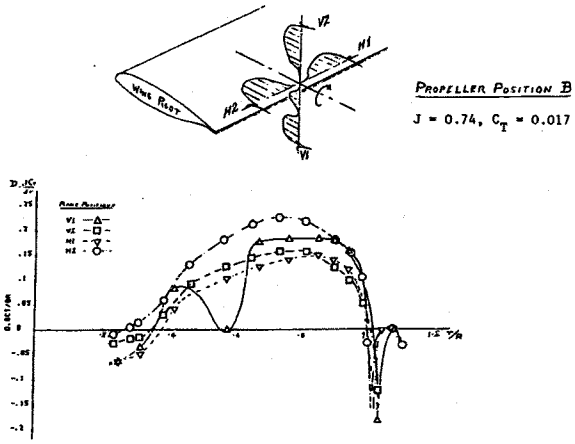

Figure 6 Thrust Grading for Propeller Position B, Low Power

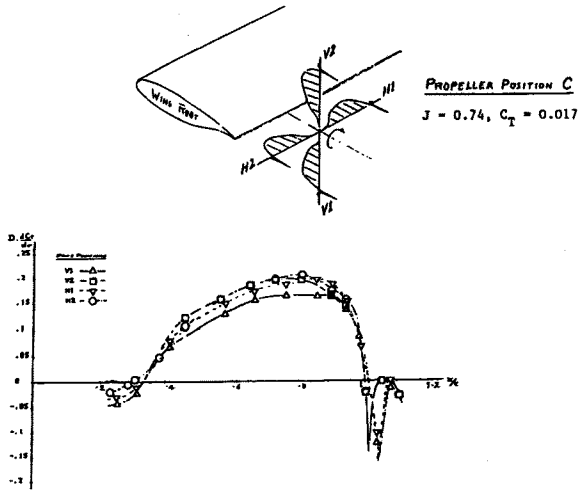

Figure 7 Thrust Grading for Propeller Position C, Low Power

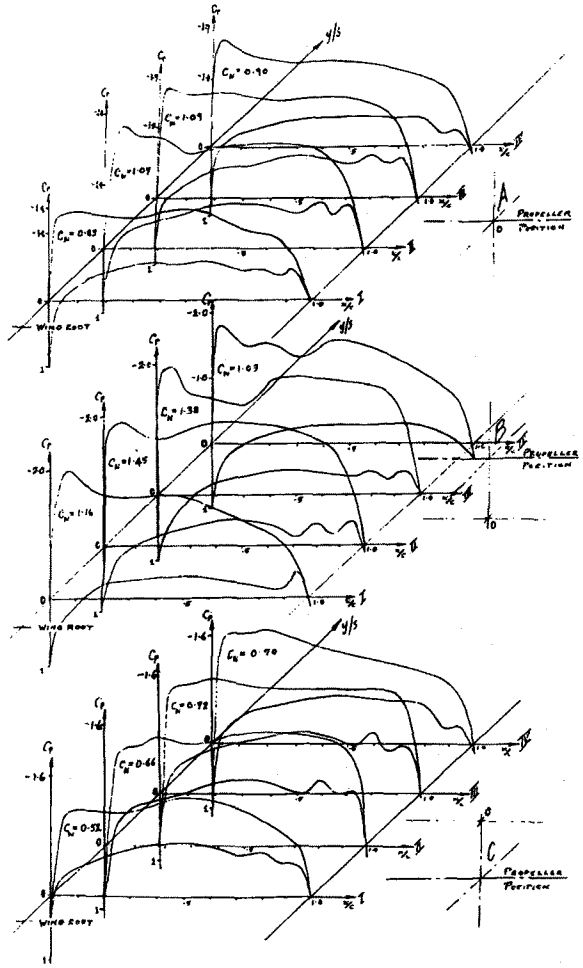

Figure 8 Pressure Distribution, Propeller Position A, B and C, High Power Case

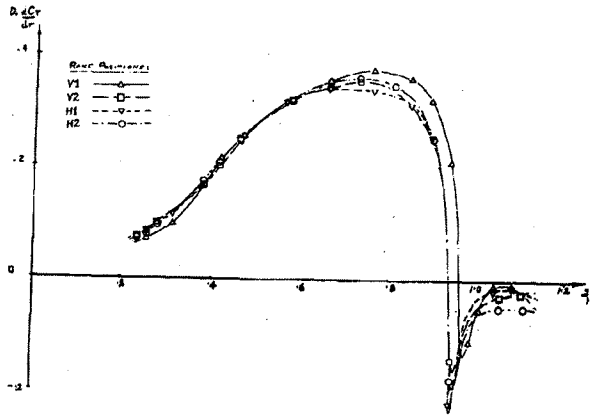

Figure 9 Propeller Thrust Grading curves for Position B High Power case

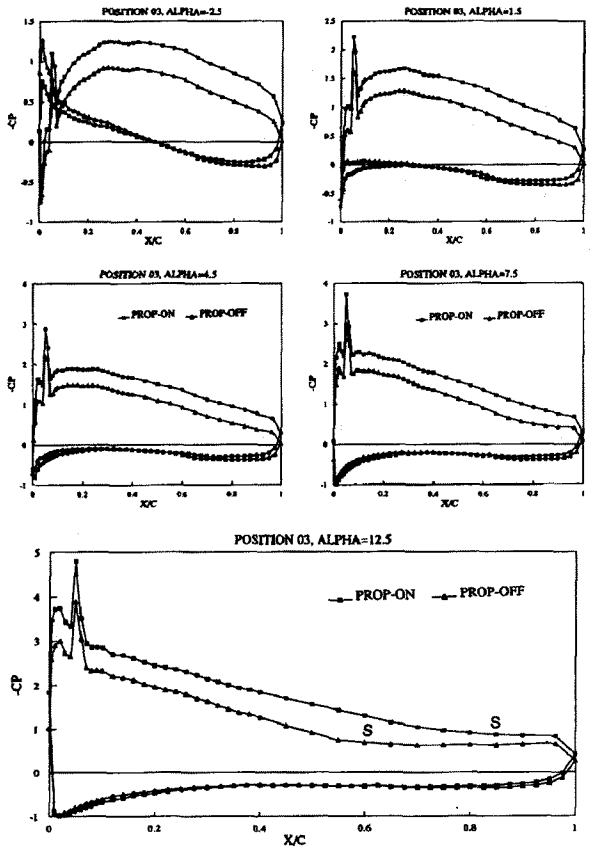

Figure 10 Pressure Distribution at the centre line of the Two-dimensional Wing (rough).

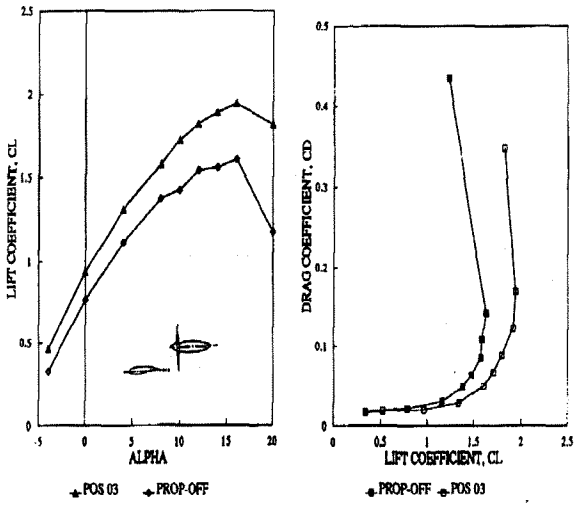

Figure 11 C_L -α , C_D - C_L Results for 2-D Wing (rough) Propeller Position 03.

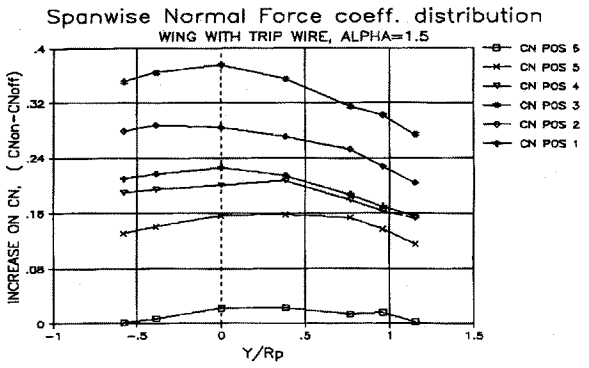

Figure 12 Spanwise normal Force Coefficient, by Integrated Pressure Distribution, Rough Wing, α=7.5°

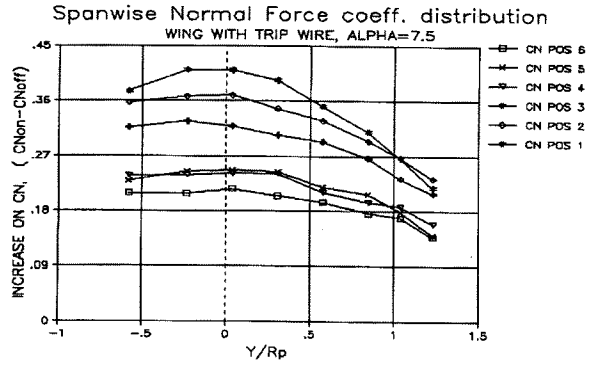

Figure 13 Spanwise normal Force Coefficient, by Integrated Pressure Distribution, Rough Wing, α=7.5°

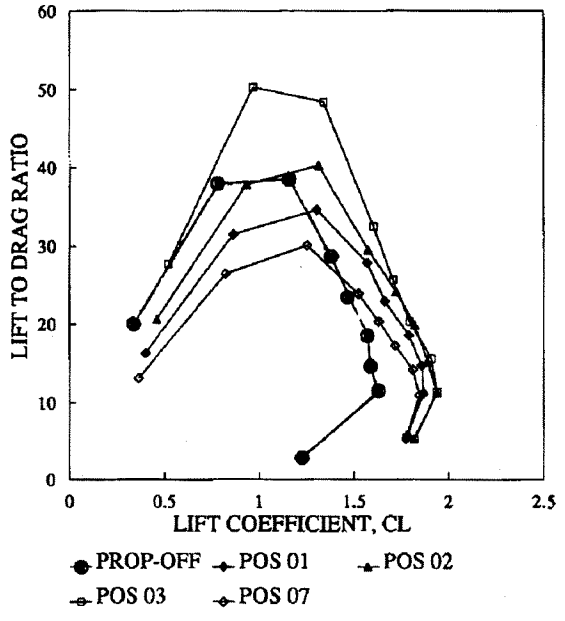

Figure 14 Lift to Drag Ratio Compared with Propeller off Case.

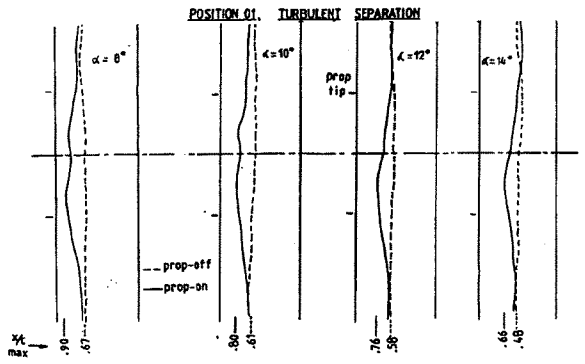

Figure 15 Turbulent Separation Front, Propeller position 01, rough wing, oil flow tests

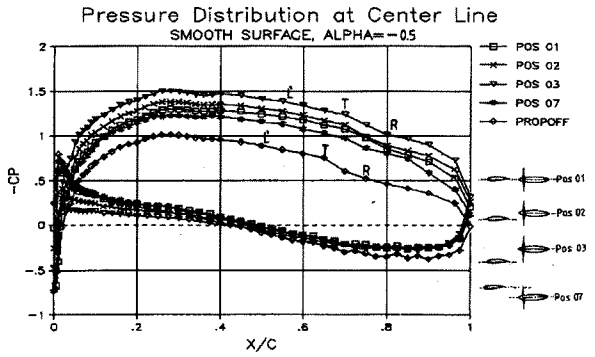

Figure 16 Pressure Distribution for the Smooth Wing

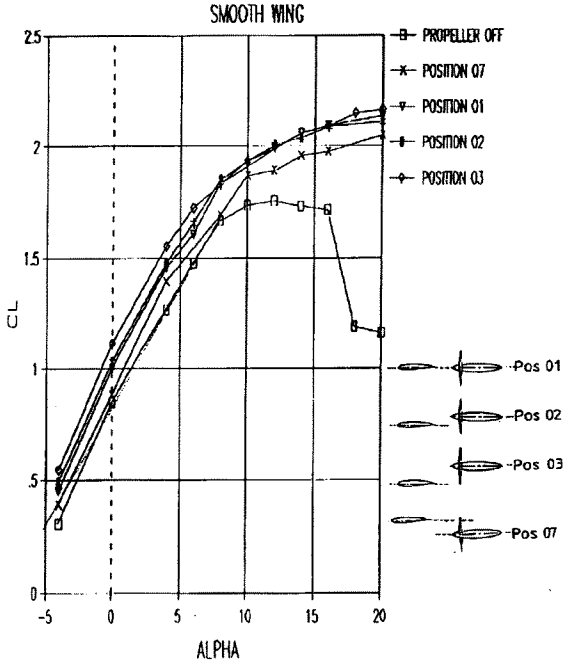

Figure 17 C_L - α For the Smooth Wing

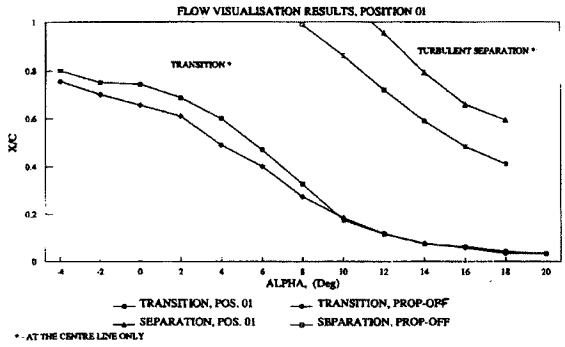

Figure 18 Transition and Turbulent Separation Points at the Centre Line of the Smooth Wing Determinated by Flow Visualization

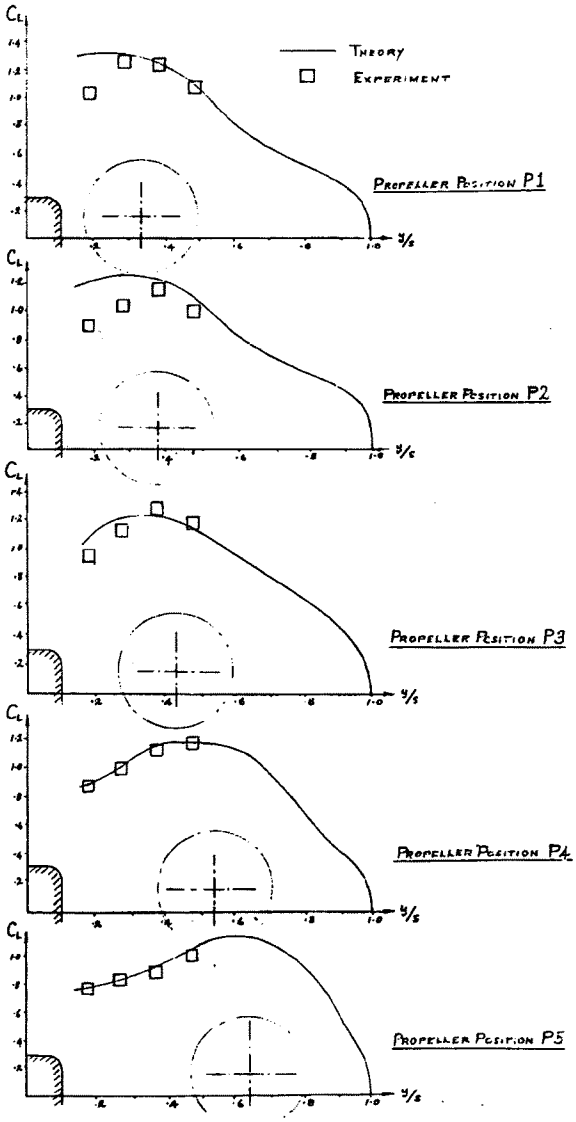

Figure 19 Spanwise Loading, High Power case, Comparison With theory .

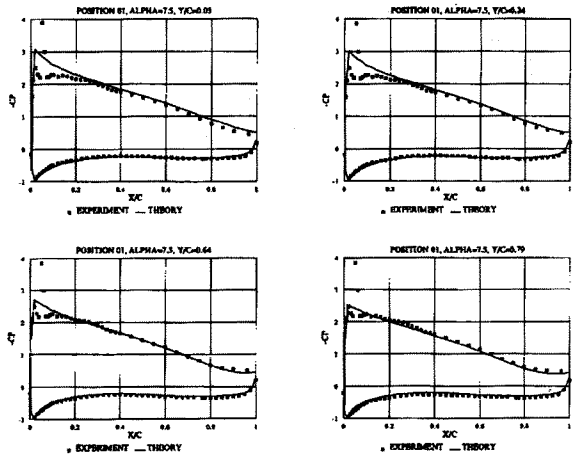

Figure 20 Comparison with Theory, rough wing, Propeller Position 01, $\alpha = 7.5^{\circ}$

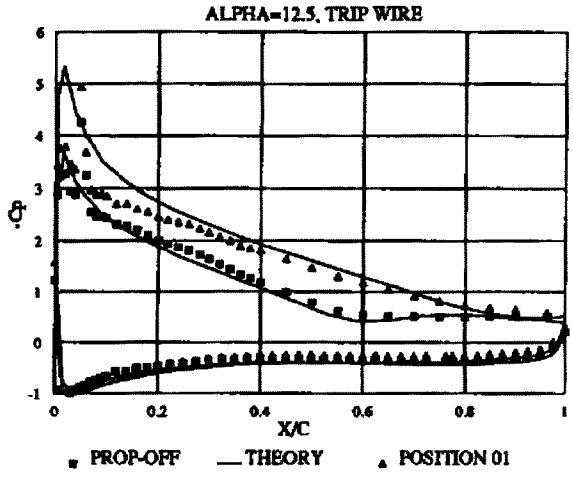

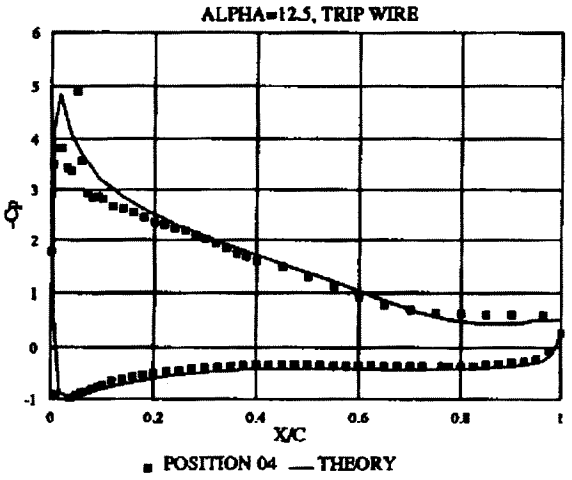

Figure 21 Comparison with Theory, rough wing, Propeller positions 01 and 04, $\alpha = 12.5^{\circ}$.

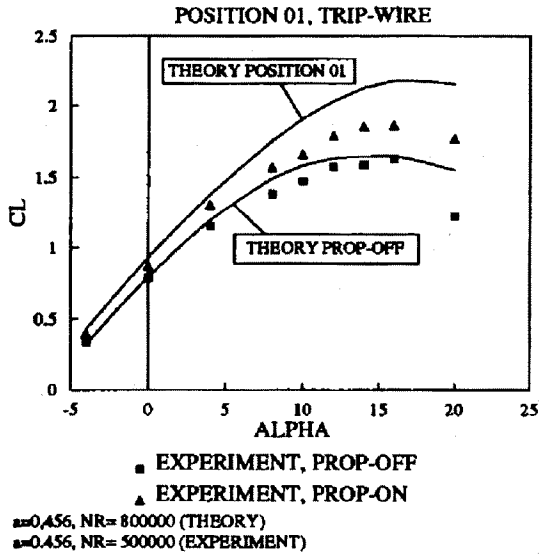

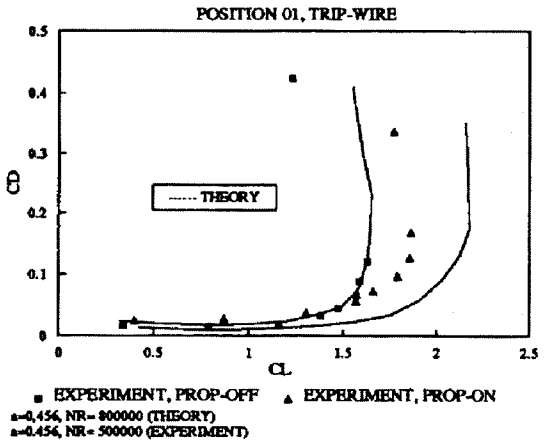

Figure 22 Integrated Spanwise distribution of calculated Lift and Drag Coefficients, position 01, comparison with theory

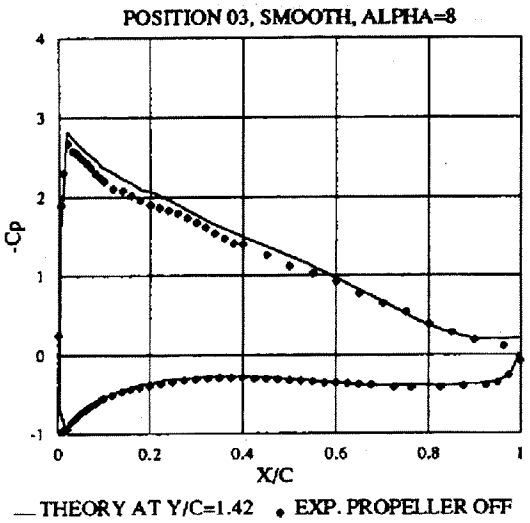

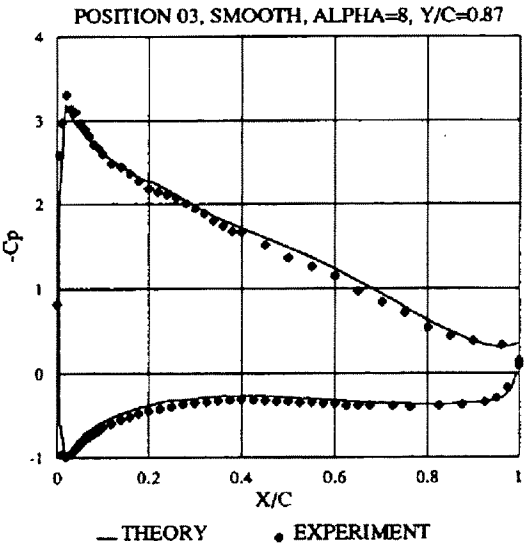

Figure 23 Pressure distribution, Smooth wing, comparison with theory, $\alpha = 8^{O}$

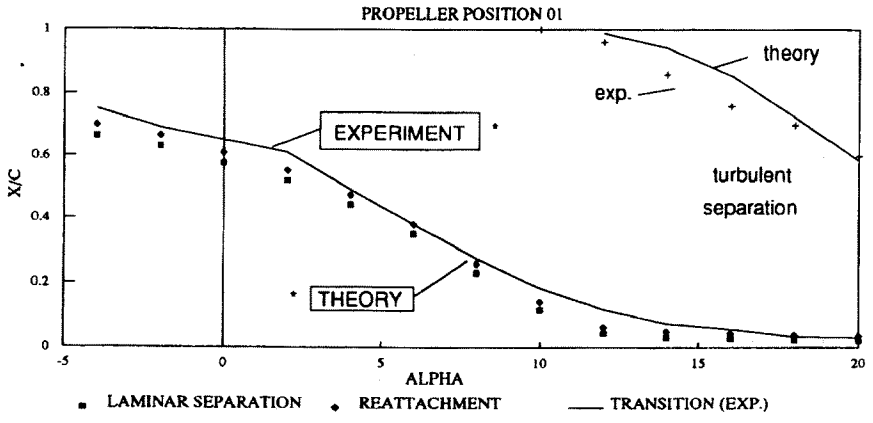

Figure 24 Comparison with theory, transition and turbulent separation at centre line, smooth wing , **position 01**